Marine Geology 448 (2022) 106802

Contents lists available at ScienceDirect

Marine Geology

journal homepage: www.elsevier.com/locate/margo

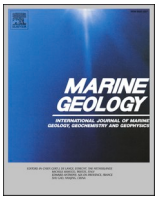

Potential and limitation of ^{230}Th-excess as a chronostratigraphic tool for late Quaternary Arctic Ocean sediment studies: An example from the Southern Lomonosov Ridge

Karl Purcell [a,b], Claude Hillaire-Marcel [a,*], Anne de Vernal [a], Bassam Ghaleb [a], Ruediger Stein [c,d,e]

[a] Geotop and Department of Earth and atmospheric sciences, Université du Québec à Montréal, Montréal H3C 3P8, Canada
[b] Department of Earth Science, University of Bergen and Bjerknes Centre for Climate Research, 5020 Bergen, Norway
[c] Center for Marine Environmental Sciences (MARUM), University of Bremen, 28334 Bremen, Germany
[d] Frontiers Science Center for Deep Ocean Multispheres and Earth System, Key Laboratory of Marine Chemistry Theory and Technology, Ocean University of China, Qingdao 266100, China
[e] Alfred Wegener Institute (AWI) Helmholtz Centre for Polar and Marine Research, Bremerhaven, Germany

ARTICLE INFO

Editor: Adina Paytan

Keywords:
Arctic Ocean
Lomonosov Ridge
Quaternary
^{230}Th-excess
U-mobility

ABSTRACT

Recently, the use of "extinction ages" of excesses in U-series isotopes ($^{230}Th_{xs}$, $^{231}Pa_{xs}$) has been proposed for the setting of benchmark ages of up to ~350 and ~150 ka, respectively, in late Quaternary marine records from the Arctic Ocean. However, the use of such U-series-based chronostratigraphic approaches has some limitations. These limitations are illustrated by U-series measurements in a cored sequence from the southern Lomonosov Ridge (PS2757). In this core, the final measurable excess in ^{230}Th ($^{230}Th_{xs}$), strictly linked to the sedimentary flux of this isotope from the overlying water column ($^{230}Th_{xs}$-marine), is observed at a depth of ~590 cm downcore. An "extinction age" of ~230 ka can be estimated for the residual $^{230}Th_{xs}$ at this depth. It approximately matches the Marine Isotope Stage 7/8 transition. Below this transition, strong redox gradients constrained by a layer enriched in organic carbon resulted in a late-diagenetic relocation of uranium leached from detrital minerals in the over- and underlying oxidized layers. This uranium relocation resulted in large amplitude radioactive disequilibria within a core section otherwise characterized by near secular equilibria between inventories of ^{238}U-series isotopes, implying an age greater than the "$^{230}Th_{xs}$-marine extinction age" for the whole section. In the overlying part of the core, the $^{230}Th_{xs}$ distribution correlates with other $^{230}Th_{xs}$-documented sequences from the Central Arctic Ocean. $^{230}Th_{xs}$ can be thus used for stratigraphic correlations between the relatively low-sedimentation rate marine sequences of this basin, over the last two or three glacial cycles, but special attention to potential diagenetic effects is recommended. Moreover, as for a given $^{230}Th_{xs}$-marine flux at the seafloor, initial $^{230}Th_{xs}$ values are broadly inversely-proportional to the sedimentation rate, the resulting estimates of $^{230}Th_{xs}$ "extinction age" vary accordingly. This variability restricts the chronostratigraphic use of $^{230}Th_{xs}$ to sequences with relatively low sedimentation rates, such as those where the initial $^{230}Th_{xs}$-marine significantly exceeds the ^{230}Th-fraction carried by detrital minerals.

1. Introduction

The setting of a robust chronostratigraphy of central Arctic Ocean sequences remains a challenge due to many factors such as low and variable sedimentation rates (e.g., Clark, 1970; Stein, 2008), conflictual interpretations of paleomagnetic records between Arctic Ocean regions (e.g., Clark et al., 1980; Darby et al., 1989; Nowaczyk et al., 1994; Stein, 2008; Xuan et al., 2012; West et al., 2021), the sporadic downcore occurrence and limited diversity of microfossil assemblages (e.g., Backman et al., 2004; O'Regan et al., 2020), and discrepancies between local and open ocean oxygen isotope stratigraphies (e.g., Ravelo and Hillaire-Marcel, 2007). Radiocarbon chronostratigraphies spanning late glacial and Holocene intervals point to recent sedimentation rates ≤1 cm/ka in several cores from the central Arctic but up to a few tens of cm/

* Corresponding author.
E-mail address: chm@uqam.ca (C. Hillaire-Marcel).

https://doi.org/10.1016/j.margeo.2022.106802
Received 5 February 2022; Received in revised form 19 April 2022; Accepted 22 April 2022
Available online 27 April 2022

ka in sites closer to the continental margin (e.g., Stein et al., 1994; Darby et al., 1997; Poore et al., 1999; Nørgaard-Pedersen et al., 2003; Polyak et al., 2004; Deschamps et al., 2018). Unfortunately, beyond ~35 ka, radiocarbon data from marine biogenic carbonates are often unreliable (see examples in O'Regan et al., 2008; Polyak et al., 2009), due to secondary carbonate precipitation through diagenetic processes (e.g., Broecker et al., 1984; Wycech et al., 2016). Beyond ~35 ka, the late Quaternary stratigraphy of Arctic Ocean sedimentary sequences was initially set from paleomagnetic data (e.g., Clark et al., 1980), but re-interpretation led to conflictual chronostratigraphies (Nowaczyk and Baumann, 1992 or Nowaczyk et al., 1994).

In this context, the use of uranium-series (U-series) isotopes has been proposed for the setting of independent time constraints (Ku and Broecker, 1965; Huh et al., 1997). For example, by using the distribution and inventories of excesses in ^{230}Th and ^{231}Pa, i.e., of the sedimentary fraction these isotopes linked to the synsedimentary U-decay in the water column (e.g., Anderson et al., 1983), Not and Hillaire-Marcel (2010) and Hillaire-Marcel et al. (2017) demonstrated that the magnetostratigraphy of Doell and Dalrymple (1966), Clark (1970, 1981), Clark et al. (1980), and Spell and Mcdougall (1992) with mm ka^{-1} sedimentation rates (SR) in the central Arctic Ocean, was more likely than the revised interpretation of Nowaczyk and Baumann (1992) and Nowaczyk et al. (1994) (see also, Jakobsson et al., 2000) used to infer cm ka^{-1} SR at the same sites.

In the present paper, we do not attempt to reconcile these conflicting Quaternary chronostratigraphies. Instead, we intend to further document the behavior of ^{230}Th excesses (^{230}Th$_{xs}$) in Arctic sedimentary sequences, aiming to constrain their use as a chronostratigraphic tool. We use cores raised from site PS2757 on the southern Lomonosov Ridge, close to the Siberian continental margin (Fig. 1). At this site, two cores, i.e., PS2757–8 (an about 8 m long gravity core) and PS2757–6 (a 35 cm-multicore) were recovered, the multicore providing an undisturbed

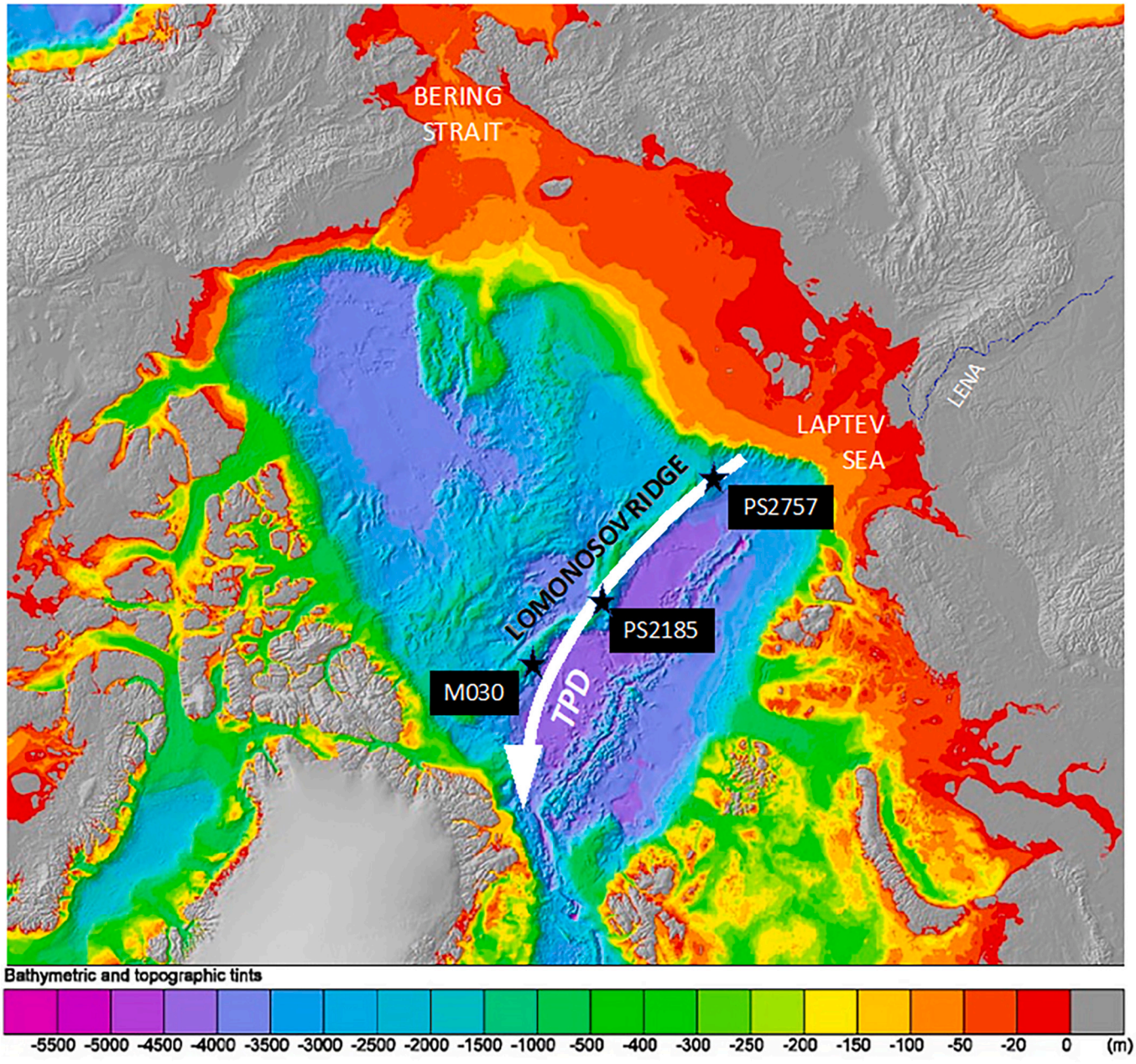

Fig. 1. Location of cores cited (black stars); white arrow: Trans-Polar Drift (TPD). The background map shows the Arctic Ocean bathymetry from Jakobsson et al. (2012).

record of the most recent sediment (Rachor, 1997). The composite record from the two cores is further on referred to as "Core PS2757". At this site, mean SR of ~1.6 cm. to 4.8 cm ka-^{1} were estimated from earlier studies based on different tentative age models (Strobl, 1998; Stein et al., 1997, 2001a, 2017a). Our objective was to test the applicability of the $^{230}Th_{xs}$ method at this site, i.e., a site with relatively high SR, in comparison with those from the central Arctic Ocean, thus, where initial $^{230}Th_{xs}$-values were likely to be much lower. Our study thus extends the work of Not and Hillaire-Marcel (2010) and Hillaire-Marcel et al. (2017) who described the $^{230}Th_{xs}$ method for sites with mm ka^{-1} SR. We also sought to characterize the behavior of U-isotopes in a sequence with intervals containing relatively elevated organic carbon contents. Such intervals may trigger the development of redox gradients in the sedimentary column and lead to a diagenetic redistribution of redox-sensitive elements such as uranium (e.g., Bonatti et al., 1971; Vallières et al., 1993), with impact on the relative distribution of ^{238}U-daughter isotopes (^{234}U and ^{230}Th in particular).

2. Materials and methods

We used sub-samples from an 8.4 m long Kastenlot core raised from the southern tip of the Lomonosov Ridge (PS2757–8: 81°09.8′ N, 140°12.0′ E, 1241 m depth; Fig. 1), previously investigated for organic-geochemical bulk parameters by Stein et al. (2001a). Based on the lithological core description, the upper ~14 cm display coring disturbances (Stein et al., 1997). Thus, in order to set a composite record for the study site, we also analyzed a multicore collected less than 3 nautical miles away (PS2757–6; 81°11.37′ N, 140°02.67′ E, 1290 m depth; 35 cm long), where the surface sediment was preserved (see details in Supporting Information section).

2.1. Sediment properties and sub-sampling

The measurements of total carbon (C_{tot}), organic carbon (C_{org}), and total nitrogen (N_{tot}), those of δ^{13}C-values of organic carbon ($\delta^{13}C_{org}$) and of U-series isotope were made in Geotop-UQAM laboratories. For this purpose, core PS2757–8 was sampled and analyzed at 20 cm intervals, and core PS2757–6 at ~5 cm intervals (see Supporting information; Tables S3 and S4). Other sedimentological, mineralogical, geochemical, and micropaleontological data cited in the present study come from earlier studies. Müller and Stein (2000) made grain size measurements using sieving/settling techniques and bulk sediment mineralogical analysis by X-ray diffraction. Heavy minerals were studied in detail by Behrends (1999). Wet bulk density changes downcore are from Niessen (1996) and were determined with a non-destructive Density Measuring System. Elemental geochemistry measurements were made using X-ray fluorescence by Schoster (2005), except for sulfur, which was analyzed with an elemental analyzer. Micropaleontological analysis was done by Matthiessen et al. (2001).

2.2. Elemental and stable isotope ($\delta^{13}C_{org}$) analysis

Total carbon (C_{tot}), organic carbon (C_{org}), and total nitrogen (N_{tot}) contents were measured using a Carlo Erba™ elemental analyzer. The measurement for C_{org} was made after fumigation with 12 M HCl to dissolve carbonates, including detrital dolomite (see Maccali et al., 2013). The isotopic composition of organic carbon ($\delta^{13}C_{org}$) was obtained on a fumigated aliquot with a Vario™ micro cube elemental analyzer connected to an Isoprime 100™ mass spectrometer. Overall analytical precision is better than ±0.1‰ for $\delta^{13}C_{org}$ (±1σ), based on measurements of replicate samples (see details in the Supporting Information).

2.3. U- and Th-series analyses

Following chemical separation as described in Edwards et al. (1987), U and Th isotopic concentrations were obtained from MC-ICP-MS measurements and converted into activities using half-lives from Cheng et al. (2013). The overall analytical reproducibility was ~ ±1% (± 2σ; see Supporting Information for details).

Inventories of U-series isotopes were calculated as follows:

$$\text{Inventory}\ \left(\text{dpm cm}^{-2}\right) = \sum_{i}^{n} X_n \text{ x } \overline{A_n} \text{ x } \overline{\rho_n}$$

where X_n (cm) is the thickness, $\overline{A_n}$ (dpm g^{-1}) is the average activity, and $\overline{\rho_n}$ (g cm^{-3}) is the average dry bulk density of the nth depth interval (Not and Hillaire-Marcel, 2010).

Between the measured depths, all values were linearly interpolated. Whereas the interpolation could result in some uncertainty, we assumed that potential negative and positive offsets should end even up when summed up across the 44 samples of the composite sequence

3. Results

3.1. Sediment properties

Core PS2757–8 is composed of brown silty clays (Stein et al., 1997) with some intervals containing up to 30% sand (Müller-Lupp et al., 2000). The average weight percentages of sand (63 μm – 2 mm), silt (2 μm – 63 μm) and clay (< 2 μm) fractions are 5.3 ± 7.1%, 46.5 ± 8.6% and 48.2 ± 11.8%, respectively (Müller and Stein, 2000); clay and sand contents are anticorrelated ($R = -0.70$; see Fig. 2). Bulk mineralogical analysis indicates that quartz (~ 43%), plagioclase (~ 24%), pyroxene (~ 10%), and alkali feldspars (~ 6%) dominate. Amphibolites, kaolinites, chlorites, smectites, and illites also exist in variable and minute quantities (Müller and Stein, 2000). Heavy minerals of the 240–600 cm interval differ from those found in the over- and underlying sediment sections, suggesting that the coarse material from this intermediate section originated from distinct sources (Stein et al., 1997; for details see also Behrends, 1999). The sequence depicts very low carbonate contents (≤ 0.2 dry weight percent -dw%-) with minor pulses matching increases in peaking sand values (Supporting Information).

3.2. Organic carbon content and isotopic composition

The organic carbon content varies between ~0.9 and ~0.1 dry weight percent (dw%) in the study sequence (Fig. 2). The maximum value is observed at the core top. It is slightly above values reported in surface sediments from northernmost sites along the Lomonosov Ridge (0.6 to 0.3 dw%; Stein and Macdonald, 2004). Below, C_{org}-values decrease within the first meter to ~0.3 dw%, then more progressively to ~0.1 dw% reached at ~5.5 m. Deeper in the core, C_{org}-values increase again within a close to 1 m-thick layer - (~ 6.2–7.2 m), peaking at ~0.7 dw%.

C_{org}/N_{total} molar ratios range from 1.9 to 9.8. They follow closely the C_{org}-content variations (Fig. 3). C_{org} shows δ^{13}C values mostly within the ~ −22.5‰ to −23.5‰ range (Fig. 3), suggesting organic matter fluxes with a strong marine source component (cf., Müller-Lupp et al., 2000; Naidu et al., 2000). In contrast, the -deep C_{org}-enriched layer, shows a large negative $\delta^{13}C_{org}$ excursion (down to ~ − 25‰), indicating significant inputs of terrestrial organic carbon at this depth (e.g., Naidu et al., 2000).

3.3. U- and Th-series isotopes

The $^{238}U/^{232}Th$ activity ratio (AR) of the composite record averages 0.61 ± 0.19 (±1σ), which is within the range reported for late Quaternary sediments from the Arctic Ocean (from ~0.6 to ~1; Hoffmann, 2009; Not and Hillaire-Marcel, 2010; Gusev et al., 2013). This AR value, however, is slightly below values reported in sediments from Russian rivers that flow into the Arctic (~ 0.76; Viers et al., 2009) but within one

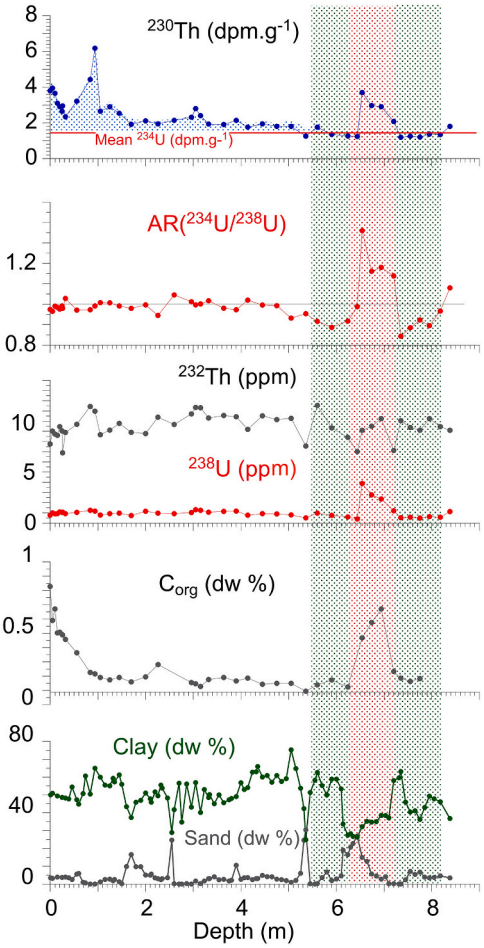

Fig. 2. Major sedimentological and geochemical properties of the composite core. The red and green vertical stripes distinguish the interval affected by late diagenetic U-relocation processes from oxidized low C_{org}-content layers (green) towards the reduced C_{org}-enriched layer (red). Green arrows on the clay and sand diagram are interpreted as glacier advances, while red arrows depict retreats (cf., Müller, 1999). The blue dotted ^{230}Th profile illustrates the decay of the initial $^{230}Th_{xs}$ above the diagenetically altered layers. The corresponding data can be found in tables S1 to S4 of the Supporting Information. (For interpretation of the references to colour in this figure legend, the reader is referred to the web version of this article.)

standard deviation of the mean Earth's crust value (e.g., Paul et al., 2003).

The mean AR(^{234}U/^{238}U) of the whole sequence averages 1.00 ± 0.09 (±1σ), with values more clustered above 560 cm (0.99 ± 0.03; ±1σ), thus suggesting near-secular radioactive equilibrium between the two isotopes at the scale of the whole sequence.

Whereas the ^{232}Th content below 560 cm downcore does not depart significantly from its value in the upper part of the core (respectively, 10.3 ± 1.12 ppm and 11.0 ± 1.0 ppm in the downcore and upcore sections; both ±1σ; Supporting Information), the uranium concentration and isotopic composition display large-amplitude variations in the lower section (Fig. 2). The top 560 cm has an average uranium concentration of ~2 ppm while a U-enriched layer, with a U-content of ~3.5 ppm and an AR(^{238}U/^{232}Th) peaking at 1.48 ± 0.01, marks the ~650–720 cm interval of the composite sequence. This U-enriched layer is over- and underlaid by U-depleted intervals (~ 590–620 cm and ~735–820 cm) marked by a U-content of ~1.6 ppm and an AR (^{238}U/^{232}Th) < 0.48. The strong peak of C_{org} values matches the U-enriched interval (Fig. 2).

Excesses in ^{230}Th scavenged from the water column were calculated

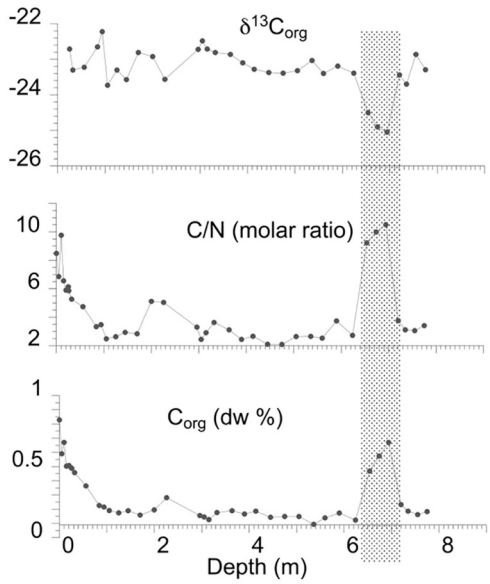

Fig. 3. Organic matter properties: A strong terrestrial carbon pulse highlighted by high C_{org}/N_{tot} ratios and low $\delta^{13}C_{org}$ -values is observed between ~6.2 and ~7.2 m with a peaking C_{org} value (grey striped layer). Other shifts in Corg content and C/N ratio (~ 2 m, and near core top) do not show a similar shift of $\delta^{13}C_{org}$ towards terrestrial values.

assuming a radioactive equilibrium between ^{230}Th (i.e., the "supported" fraction) and ^{234}U in the detrital fraction (see Supporting Information for calculation details). $^{230}Th_{xs}$-values display a broad exponential decay trend towards the core bottom (Fig. 2). Over this trend, oscillations in $^{230}Th_{xs}$ are observed, with notable peaks centered at the surface, ~1 m, and ~3 m, to be discussed below.

4. Discussion

4.1. Major sedimentological features

Sedimentological features of the study core have been reported and discussed previously (e.g., Niessen, 1996; Stein et al., 1997, 2001a, 2001b, Stein et al., 2017a, 2017b; Strobl, 1998; Behrends, 1999; Müller, 1999; Fahl and Nöthig, 2007). Here, we will focus on a few features relating to the U-series isotope behavior in the sedimentary column. Down to ~560 cm, core PS2757 presents features, not unlike those described for many other Arctic Ocean sedimentary sequences, with finer layers of elevated $^{230}Th_{xs}$ alternating with coarser $^{230}Th_{xs}$-depleted intervals (Fig. 2). These layers are usually interpreted as being deposited by sea-ice rafts and icebergs, respectively (Fig. 2), although this simplistic distinction should be used with some caution (e.g., St. John, 2008). With their progressive increase in sand content (Fig. 2), it is likely that several coarse layers have been deposited by icebergs during glacial advances, possibly over shelves under lowering sea-level conditions (cf., Müller, 1999).

The layer ranging 6.2–7.2 m downcore presents very distinct features. It depicts an elevated organic matter content, mostly from continental sources, as indicated by the relatively high C_{org}/N_{tot} ratio (up to ~12), and low $\delta^{13}C_{org}$ -values, peaking below −25‰ (Fig. 3; cf. Naidu et al., 2000). This interval of significantly elevated C_{org} contents relates to an increased supply of terrigenous organic compounds identified and correlated between sites from southern Lomonosov Ridge and the Laptev Sea continental margin by Stein et al. (2001a, 2017a). These continental materials could have been deposited during periods of enhanced riverine fluxes, but more likely reflect the erosion of organic matter-rich continental deposits during a glacial advance. This hypothesis is supported by the increase in sand content, peaking slightly above the

C_{org}-enriched layer (Fig. 2), and noting that supplies of organic matter by the Lena River are typically in the form of dissolved compounds (C/N ~ 50, Lara et al., 1998; $\delta^{13}C_{org}$ ~ −27‰; Kutscher et al., 2017). Particulate carbon from circum-Arctic peats presents isotopic compositions within the range or slightly below that of the C_{org} in the 6.3–7.3 m layer (Gusev et al., 2013). Assuming a background $\delta^{13}C_{org}$ signal of ~ −23‰ for the "marine-dominated" section of core PS2757 (Fig. 3), the peak at −25‰ in the deep organic-enriched layer would imply mixing with ~50% or more carbon from terrestrial-source (for more detailed discussion about the input and characteristics of terrigenous organic carbon we refer to Fahl and Stein, 1999; Stein et al., 2001a; Stein and Fahl, 2004)

The organic matter properties near the core top are also noteworthy. Its C_{org} content and C/N ratios are strongly correlated. Again, these signals may reflect inputs of terrestrial organic matter. However, while $\delta^{13}C_{org}$ values near the core top show relatively large amplitude variations, their mean value remains close to −23‰, which is well above that observed in the C_{org}-enriched deep layer. A particular organic matter source here could be kelp forests (with $\delta^{13}C_{org}$ values ranging −13.6 to −16.5‰ Naidu et al., 2000) that may contribute significantly to primary production in coastal waters (Dankworth, 2016). However, while Naidu et al. (2000) did not observe any significant influence of such a carbon source in surface sediments from Russian shelves, Goñi et al. (2013) did observe $\delta^{13}C_{org}$ and C_{org}/N_{tot} values in sediments from the North American Arctic margin within the range observed in the core top organic matter analyzed here.

4.2. Diagenetic behavior of uranium

Using $^{230}Th_{xs}$ to set time constraints implies a chemical closure for the parent U-isotopes since the deposition of the sediment. This condition is broadly satisfied for most low-C_{org} content, and thus oxidized sedimentary sequences of the central Arctic Ocean cited above. In the present case, some diagenetic U-mobility is observed below 560 cm downcore, in relation to the C_{org}-enriched layer. This process must be fully addressed in order to differentiate potential residual excesses in ^{230}Th derived from ^{230}Th fluxes in the water column, i.e., from $^{230}Th_{xs}$-marine, vs ^{230}Th excesses linked to diagenetic U-isotope redistribution.

At least down to 560 cm, any significant early diagenetic U-uptake of marine uranium (e.g., Gariepy et al., 1994) may be discarded, as ^{234}U and ^{238}U are in secular equilibrium (AR ($^{234}U/^{238}U$) = 0.99 ± 0.03; ±1σ) within uncertainty). Below 560 cm, the large amplitude variations in U-concentration, AR($^{234}U/^{238}U$), and AR($^{230}Th/^{234}U$) highlight an important late diagenetic U-mobility linked to redox gradients driven by the high organic carbon content of the ~650–720 cm interval (Fig. 2). All redox-sensitive elements show similar fluctuations within this interval. Manganese, Fe, V, P concentrations, and Mn/Fe molar ratios depict low values, whereas sulfur concentrations show increasing values peaking at ~0.2 dw% at ~685 cm, relative to a mean concentration of 0.071 ± 0.04 dw% in the over- and underlying sediments (Fig. 4; see also Schoster, 2005).

At least two distinct processes are recorded in the 650–720 cm interval: 1) specific sedimentary fluxes marked by the presence of terrestrial organic carbon and minor increases in inorganic carbon (see Table S2 in Supplementary Information); 2) an early-to-late diagenetic redistribution of redox-sensitive elements related to the reduced C_{org}-enriched layer vs the over and- underlying oxidized sediments (e.g., Thomson et al., 1995).

It is noteworthy that the lowering sea level and the emergence of shelves accompanying the ice advance marked by the sharp increase in sand content of the 650–720 cm layer, also led to a decrease in the important manganese oxide fluxes from shelves to the deep Arctic Ocean (e.g., Löwemark et al., 2014; Macdonald and Gobeil, 2012). These processes potentially impacted the budget of several related elements, such as uranium (e.g., Wang et al., 2013).

Similarly, in contrast with the unvarying AR($^{234}U/^{238}U$) observed above 560 cm, the U-enriched layer shows a strong excess in ^{234}U, with

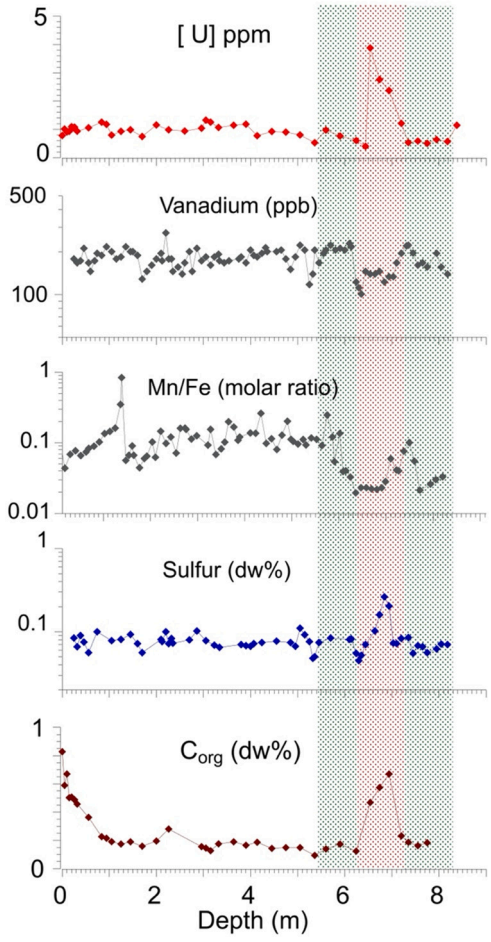

Fig. 4. Behavior of a few redox-sensitive elements in relation with the deep C_{org}-enriched layer. Vertical stripes are similar to those indicated in Fig. 2: in green, U-leaching of detrital minerals; in red: secondary U precipitation. (For interpretation of the references to colour in this figure legend, the reader is referred to the web version of this article.)

an AR($^{234}U/^{238}U$) up to 1.366 ± 0.014, whereas the immediately under- and overlaying U-depleted layers are characterized by deficits in ^{234}U, with an AR($^{234}U/^{238}U$) as low as 0.843 ± 0.004 (see Fig. 2). These signals suggest U-leaching from minerals of the oxidized layers with preferential mobility of ^{234}U over ^{238}U. This relates to the alpha-recoil of ^{234}Th following the disintegration of its parent ^{238}U, leaving the subsequent ^{234}U in a damaged lattice (Ku and Broecker, 1965). In particles with a size of 0.7 μm, 30% of the ^{234}U produced could be ejected in the pore water of pelagic sediments (Kigoshi, 1971). Accordingly, the ^{234}U-daughter isotope ^{230}Th depicts a strong excess in the U-depleted layers and a deficit in the U-enriched layer. This U-transfer process reflects a slow and long-duration diagenetic evolution, possibly still active today, that prevents the return to secular equilibrium between ^{230}Th and ^{234}U. Driven by redox gradients, U-leaching of detrital minerals from oxidized layers and its subsequent precipitation in a low Eh layer have been reported in various settings, including the turbidite sequences of the North Atlantic for total uranium (Colley et al., 1989) and with preferential ^{234}U mobility (Colley et al., 1984), and between glacial/interglacial sedimentary deposits from the Labrador Sea (Vallières, 1997).

In the Labrador Sea sequence, the oxidized glacial layers show deficits in ^{234}U (vs ^{238}U) increasing with time, from an AR($^{234}U/^{238}U$) of ~0.90 in marine isotope stage 2 (MIS 2), to ~0.88 (MIS 4) and ~0.85 (MIS 6) (Vallières, 1997), and illustrating the long-duration of these redox-driven diagenetic U-relocation processes. Worthy of mention here is the fact that the diagenetic behavior of U-series isotopes may have an

impact on the estimate of the environmental dose rate values used for Optically Stimulated Luminescence (OSL) dating, in particular of quartz, in comparison with feldspars (e.g., Zhang and Li, 2020). Adding the decay of $^{230}Th_{xs}$ through time and the diffusion of radium and radon through the sedimentary sequence, OSL-ages such as those calculated by West et al. (2021) for a site nearby PS2757, are open to debate.

4.3. Uranium mobility in the section below 560 cm

Whereas the near-equilibrium AR($^{234}U/^{238}U$) observed down to 560 cm indicates a negligible, if any, synsedimentary to early diagenetic marine U uptake in the sediment, its occurrence during or slightly after the deposition of the high C_{org} content layer cannot be discarded. First, the inventory of ^{238}U and ^{232}Th activities measured in the 13 samples analyzed within the 560–840 cm interval yields a cumulative activity ratio of ~0.72 between these two isotopes, a ratio higher than the ~0.56 value calculated from their inventory in the overlying sedimentary sequence (Table S3; Fig. 5). Second, the cumulative activities of ^{234}U and ^{238}U below 560 cm yield an AR($^{234}U/^{238}U$) value of ~1.04, i.e., a value statistically greater than the mean AR($^{234}U/^{238}U$) of the 0–560 cm sequence (0.99 ± 0.03). On this ground, one cannot discard an early diagenetic addition of marine U to the C_{org}-enriched layer sediment. However, assuming an AR($^{234}U/^{238}U$) value of ~1.14 (e.g., Chen et al., 1986) for this uranium, a ~30% contribution of marine U to the total uranium content of the 560–840 cm layer would be required to reach the observed value. This amount is well above the ~10% total excess in uranium of this layer, as estimated from its mean U-concentration (~ 2.23 ppm) in comparison with that of the overlying sedimentary column (~ 2.00 ppm; Supporting Information).

The partitioning of the U from the U-enriched layer suggests a possible contribution of another source. Let us hypothesize that detrital minerals of the interval below 560 cm are characterized by a [U/Th] molar ratio and U-isotope compositions similar to those of the 0 to 560 cm interval. The isotopic composition of the ~0.23 ppm uranium in excess (U_{EXCESS}), as calculated above, compared to that of the 2 ppm detrital fraction ($U_{DETRITAL}$), would be as follows:

$$U_{EXCESS} = U_{DEEP-LAYER} - \left[(U/Th)_{DETRITAL} * Th_{DEEP-LAYER}\right]$$

Where:
$U_{DEEP\text{-}LAYER}$ = total ^{238}U-inventory in dpm cm^{-2} below 560 cm
$Th_{DEEP\text{-}LAYER}$ = ^{232}Th-inventory in dpm cm^{-2} below 560 cm
$(U/Th)_{DETRITAL}$ = mean AR($^{238}U/^{232}Th$) of the 0 to 560 cm interval
Then,

$$^{238}U_{EXCESS} = {}^{238}U_{DEEP-LAYER} - \left[\left(^{238}U/^{232}Th\right)_{DETRITAL} * {}^{232}Th_{DEEP-LAYER}\right]$$

$$= \sim 517 \text{ dpm cm}^{-2} - [\sim 0.558 * 779 \text{ dpm cm}^{-2}] = \sim 82 \text{ dpm cm}^{-2}$$

$$^{234}U_{EXCESS} = {}^{234}U_{DEEP-LAYER} - \left[\left(^{234}U/^{232}Th\right)_{DETRITAL} * {}^{232}Th_{DEEP-LAYER}\right]$$

$$= \sim 552 \text{ dpm cm}^{-2} - [\sim 0.551 * 779 \text{ dpm cm}^{-2}] = \sim 122 \text{ dpm cm}^{-2}$$

This calculation yields an AR($^{234}U/^{238}U$) of ~1.49 for the uranium in excess in the deep layer, a value much higher than that of marine uranium (~ 1.14; e.g., Chen et al., 1986). Thus, if some marine U could have been taken up during sedimentation and the subsequent early diagenetic phase, another source of ^{234}U-enriched U must be found.

Given the continental signature of the C_{org} accumulated in the 650–720 cm section, sediment sources with distinct U-concentrations and activity ratios should be considered first. As illustrated in Fig. 2, this C_{org}-enriched layer matches an increase in the sand fraction that we linked to ice advance over shelves, with a lowering sea level (cf., Müller, 1999; Stein et al., 2001a). During this ice margin advance, incorporation of material from Arctic soils and/or peat-bog both with high U contents and excesses in ^{234}U above ^{238}U (e.g., Łokas et al., 2019; Frechen et al., 2007), was likely the process responsible for the high AR($^{234}U/^{238}U$) inferred for the additional uranium content of the layer. Sediments from Bolshoy Lyakhovsky Island in Russia, ~ 860 km south of the study sites, provide an example of such C_{org}-enriched sediment sources with a high U-content and with an AR($^{234}U/^{238}U$) value as high as 1.415 (Schirrmeister et al., 2002; see also Allard et al., 2012).

The deepest sample analyzed in the study core (Supplementary Information) indicated a near secular equilibrium between ^{230}Th and ^{234}U but still depicts a slight excess in ^{234}U relative to ^{238}U. Diagenetic processes or a residual ^{234}U-excess inherited from the deposition of ^{234}U-enriched detrital sediment could be evoked. In the first case, the secular equilibrium between ^{230}Th and ^{234}U suggests that any diagenetic U-flux would have been so slow that it would not result in any measurable deficit in ^{230}Th. In the second case, the depositional age of the sample should exceed the $^{230}Th_{xs}$-time window under such settings (see below) but would still be within a measurable detrital ^{234}U-excess decay range (≤ 1 Ma).

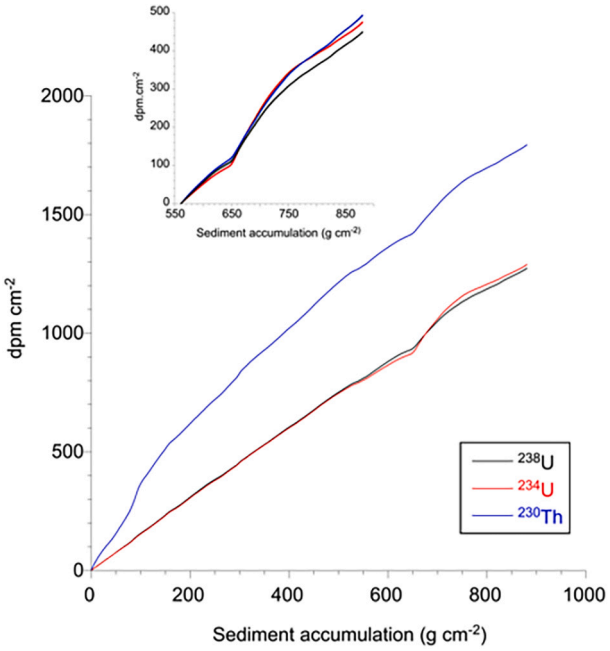

Fig. 5. Inventory of ^{230}Th, ^{234}U, and ^{238}U activities downcore. Insert: Inventories in the 560–840 cm section affected by diagenetic U-relocation processes. The near radioactive equilibrium between ^{230}Th and ^{234}U in the bottom 560–840 cm section suggests that the initial $^{230}Th_{xs}$ has broadly decayed within uncertainties of its calculated value in this layer, and thus that U-relocation occurred at very slow rates or back in time during a period beyond 5/6 half-lives of ^{230}Th.

4.4. Chronological constraints from $^{230}Th_{xs}$ distribution and decay

Below 560 cm, the inventory of ^{230}Th activity matches that of ^{234}U with an offset of ~ +0.05% (Table S3; Fig. 5). No significant cumulative $^{230}Th_{xs}$ is thus observed within the deep layer, despite its large amplitude fluctuations linked to the diagenetic processes discussed above.

Regardless of the uncertainty about the initial $^{230}Th_{xs}$-marine of this deep layer, one may assume an age beyond the "extinction age" of the $^{230}Th_{xs}$ component (cf. Hillaire-Marcel et al., 2017). This "extinction age" is reached when the $^{230}Th_{xs}$ falls within the error bars of the difference between total ^{230}Th and its supported fraction, where (^{234}U) is assumed to represent this supported fraction, i.e., when $^{230}Th_{xs} \sim (\sigma(^{230}Th)^2 + \sigma(^{234}U)^2)^{0.5}$. In the present case, we used the mean ^{234}U activity and standard deviation in the 0–560 cm section (1.49 ± 0.11 dpm g^{-1}; ±1σ; $n = 29$) as an estimate of the supported fraction and the uncertainty of its value. Calculating an age for the sedimentary layer where $^{230}Th_{xs}$ falls within error bars of its calculated value requires

knowing the initial $^{230}Th_{xs}$ of this layer. Under steady-state conditions (i.e., with constant sedimentary and $^{230}Th_{xs}$-marine fluxes), the distribution of $^{230}Th_{xs}$ downcore should follow a negative exponential function. As illustrated in Fig. 6, $^{230}Th_{xs}$-values decrease downcore and broadly follow an exponential decay pattern. However, with the known variability of SR in the Arctic Ocean and the variability of other processes governing $^{230}Th_{xs}$ scavenging and sedimentary accumulation (e.g., Hillaire-Marcel et al., 2022), one cannot link the residual $^{230}Th_{xs}$ of any specific layer to a given initial $^{230}Th_{xs}$-activity. Nevertheless, the overall trend may be used to estimate the statistical boundaries of the approximate age of this "extinction age" as plotted with a logarithmic y-scale in Fig. 6. With a 68% probability, an age of 231 + 31/−25 ka is obtained at a depth of ~5.9 ± 1.5 m. Given the near $^{230}Th/^{234}U$-equilibrium below 590 cm, as suggested by their inventories, the most probable depth of the $^{230}Th_{xs}$ "extinction" would thus have to be within the ~440–590 cm interval.

4.5. A $^{230}Th_{xs}$-stratigraphy

The $^{230}Th_{xs}$ flux on the seafloor of the Arctic Ocean cannot be interpreted conventionally (e.g., Hillaire-Marcel et al., 2022 vs Costa et al., 2019). The scavenging of $^{230}Th_{xs}$ by particles and compounds occurs at uneven rates, sporadically, and during very short time intervals. During glacial periods, scavenging rates can be practically non-existent below multiyear sea ice or ice shelves but may resume during ice streaming and surging events. Such events may last from a few hundred years (Kleman and Applegate, 2014) to a couple of thousand years in the case of major surging events (Veiga-Pires and Hillaire-Marcel, 1999; Ziemen et al., 2019). Moreover, coarse particles carried by icebergs are not efficient scavengers as most of the $^{230}Th_{xs}$ is scavenged by clays and colloidal compounds (Roy-Barman et al., 2005; Baskaran et al., 1992). Consequently, there is no effective mechanism leading to any significant and steady $^{230}Th_{xs}$ accumulation during glacial stages, as illustrated by sedimentary gaps in the central Arctic Ocean during the last glacial maximum (e.g., Not and Hillaire-Marcel, 2010). During such intervals, $^{230}Th_{xs}$ is exported towards the Nordic Seas through intermediate and deep-water circulation (Hoffmann et al., 2013; Hillaire-Marcel et al., 2017). Some ^{230}Th build-up in the water column may be hypothesized under sluggish deep-water circulation

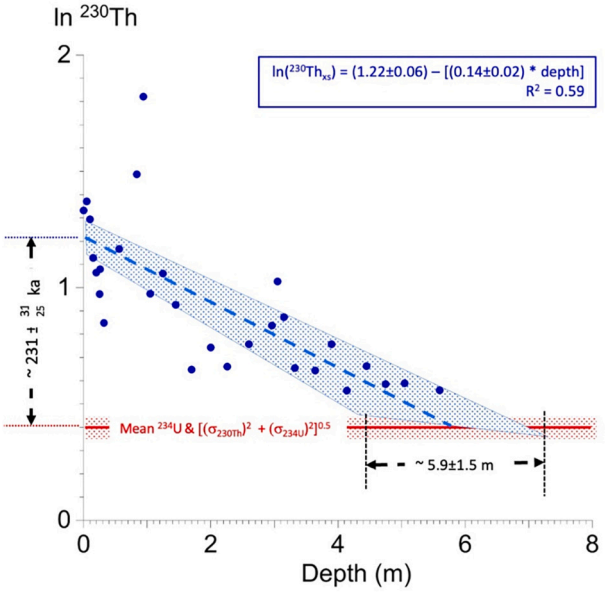

Fig. 6. Plot of ln^{230}Th downcore vs the uncertainty of its estimate from the mean ^{234}U-activity assumed to represent the supported fraction of ^{230}Th, inherited with detrital minerals. The age of the $^{230}Th_{xs}$ "extinction" and its depth are calculated with a ± 1σ probability.

conditions (Grenier et al., 2019; Kipp et al., 2021). These conditions could have prevailed during MIS 4, an interval during which very low to negligible $^{230}Th_{xs}$-values were recorded (e.g., Geibert et al., 2021). During the early MIS 3, on the other hand, sediments are characterized by peaking values, as discussed below.

During interglacials periods and some interstadials marked by high sea levels, Arctic shelves were submerged allowing the development of sea-ice factories (de Vernal et al., 2020). $^{230}Th_{xs}$ scavenging and $^{230}Th_{xs}$ fluxes to the seafloor were then driven by a large array of factors: the seasonal sea-ice growth and melt, the brine production and sinking, the development of a strong halocline with possible isopycnal transport of $^{230}Th_{xs}$ (e.g., Pavia et al., 2020), the enhanced marine production and turbidity on the shelves, and the sea-ice rafting routes (cf. Hillaire-Marcel et al., 2017). However, seasonally open sea-ice conditions over shelves did not encompass the full duration of interglacial and interstadial stages but seem to characterize relatively short time windows, as illustrated by Holocene records from the Lomonosov Ridge (de Vernal et al., 2020) and the Eurasian continental margin (e.g., Hörner et al., 2016; Stein et al., 2017b). The consequences are twofold: 1) $^{230}Th_{xs}$ accumulation mostly occurs under high detrital and particulate/dissolved organic matter fluxes linked to sea-ice rafting and brine sinking; 2) gaps alternating with highly variable fluxes are linked to sporadic sedimentary pulses. These highly variable $^{230}Th_{xs}$ fluxes result in a non-constant proportionality between ^{230}Th production in the water column, its scavenging and deposition rates, and time (e.g., Hillaire-Marcel et al., 2022). Whereas the last glacial maximum sedimentary gap that characterizes many sites from the central Arctic Ocean may illustrate conditions under full glaciation, the peaking $^{230}Th_{xs}$ sedimentary fluxes during the early MIS 3 illustrates conditions during a short interval of seasonally open sea ice conditions following the MIS 4-gap (Geibert et al., 2021). This MIS 3 peak is observed systematically in all Arctic Ocean cores (Not and Hillaire-Marcel, 2010; Gusev et al., 2013; Hillaire-Marcel et al., 2017; Geibert et al., 2021). It may be dated at ~55 ka, combining radiocarbon chronologies, age estimates of a corresponding high sea level (e.g., Siddall et al., 2008), open conditions in the Bering Strait (Farmer et al., 2021), and peaking insolation during this time window (cf. Hillaire-Marcel et al., 2022). These conditions would have permitted the development of sea-ice factories over shelves.

The above features explain the great variability of $^{230}Th_{xs}$-recordings in the Arctic Ocean and document the difficulties in using this isotope to set any reliable "radiometric age", other than that of the final "extinction age" documented above. However, $^{230}Th_{xs}$ profiles can be correlated between sites as documented earlier by Not and Hillaire-Marcel (2010) and observed later by other authors (Hillaire-Marcel et al., 2017; Geibert et al., 2021). On this ground, a $^{230}Th_{xs}$-stratigraphy is proposed with peaking $^{230}Th_{xs}$ values during MIS 1, 3, 5e, and 7 (Fig. 7), superimposed over the broad negative exponential trend illustrated in Fig. 6 for core PS2757.

Sedimentary fluxes from ice-rafted debris show an inverse relationship with the distance from the sediment sources area, in the Laptev Sea, along the TPD route (Figs. 8, 1). Such a general decrease in terrigenous (as well as biogenic) sediment fluxes towards the central Arctic Ocean has been documented in several other studies (e.g., Polyak et al., 2009; Stein et al., 2010).

The $^{230}Th_{xs}$ fluxes show reduced variability but differ sufficiently, despite the nearly similar water depths, to further illustrate the particularity of scavenging processes in the Arctic Ocean. Aside from the impact of advection and focusing processes relating to current circulation patterns (e.g., Francois et al., 2004), other parameters govern $^{230}Th_{xs}$ fluxes in this ocean (e.g.: Hillaire-Marcel et al., 2017), in particular, i) the production rate of organic matter in sea ice, and its impact on $^{230}Th_{xs}$ scavenging, ii) the production rate and sinking pattern of brines, iii) sea ice rafting routes. These processes and their impact on the cycling of $^{230}Th_{xs}$ at the basin scale still require further investigation.

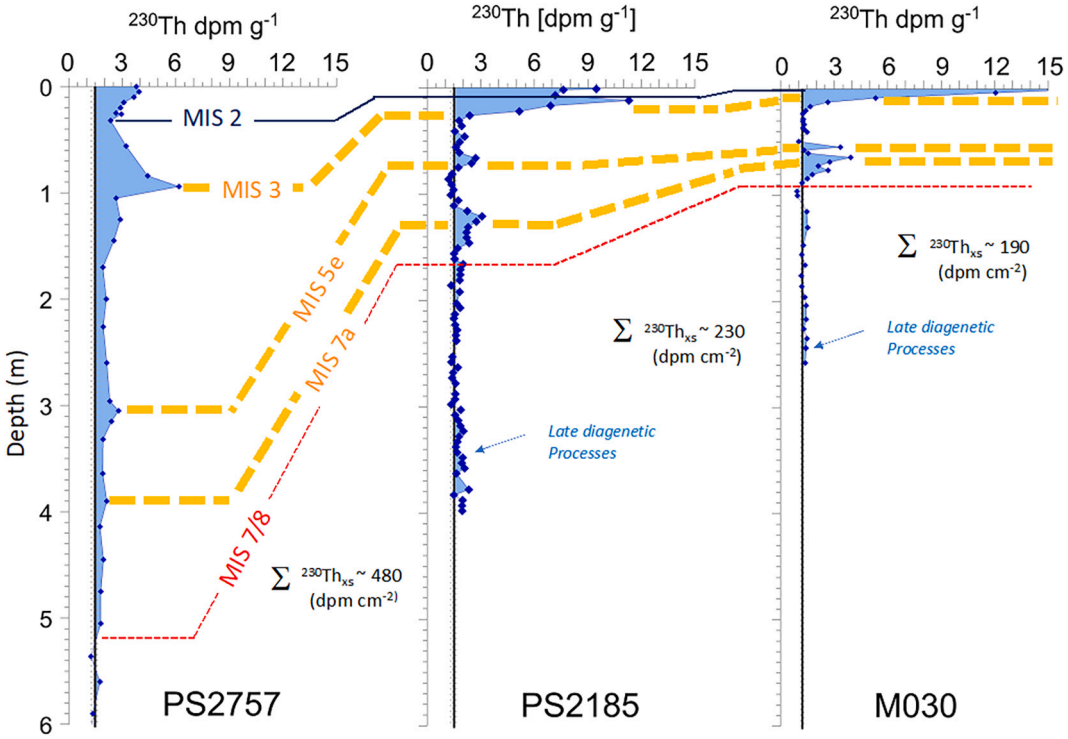

Fig. 7. Correlation of $^{230}Th_{xs}$ profiles in cores from the Lomonosov Ridge (from the south at left to the north on the right) with their tentative stratigraphic assignments (MIS = Marine isotope stages). All cores are within a narrow water depth range. Whereas sedimentation rates vary by nearly one order of magnitude, $^{230}Th_{xs}$ inventories (Σ) vary by a factor of ~2 between the two extreme sites. Note the peaking $^{230}Th_{xs}$-value of MIS 3 at all sites, and the "background noise" of minute $^{230}Th_{xs}$ values observed in sections below the "$^{230}Th_{xs}$-extinction depth", relating to long-duration late diagenetic processes (see text).

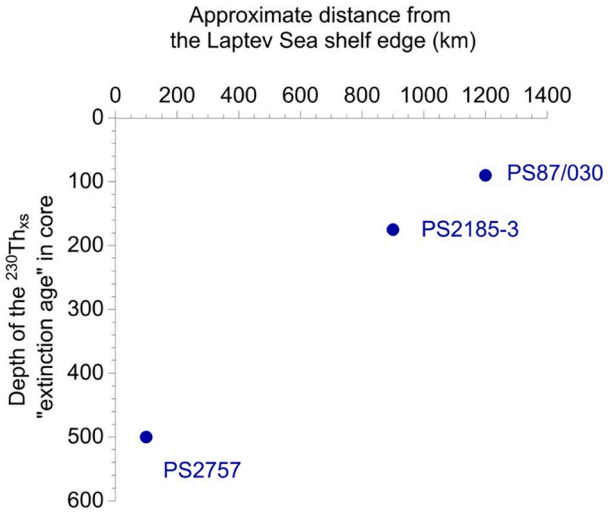

Fig. 8. The approximate distance between the coring sites shown in Fig. 1, along the Lomonosov Ridge, from the edge of the Laptev Sea shelf, versus the extinction depth of $^{230}Th_{xs}$ in the corresponding cores. Situated below the TPD route, these sites illustrate a decreasing trend in ice-rafting deposition northward from the shelf where sediment uploading takes place.

5. Conclusion

Compared with other sites in the central Arctic Ocean, our study site on the Southern Lomonosov Ridge, provides an improved resolution for the documenting of $^{230}Th_{xs}$ fluctuations during the last couple of climatic cycles (e.g., Geibert et al., 2021). This resolution allowed us to clearly distinguish the Holocene vs the MIS 3 $^{230}Th_{xs}$-peaks, which are often merged in records from very low sedimentation rate sites. However, quantifying an effective "$^{230}Th_{xs}$ extinction age" was challenging in core PS2757, in comparison with lower SR sites. The enhanced SR of site PS2757 resulted in the mixing of $^{230}Th_{xs}$ within a larger sediment mass, thus lowering the resolution of its measurement over the supported fraction. Consequently, the "extinction age" of $^{230}Th_{xs}$ calculated at the site is much younger than that proposed for lower sedimentation rate sites and marked by a much larger depth, and thus time uncertainties.

Site PS2757 also provided a well-documented record of the diagenetic mobility of uranium in sediments, linked to redox gradients. This mobility was reduced in the low organic carbon content sediments of the central Arctic Ocean. Here, we see that a few tens of a percent more C_{org} (from terrestrial fluxes linked to a glacial advance) led to a redistribution of redox-sensitive elements, such as uranium, in the deepest section of the core. Therefore, the use of the excesses in U-series daughter isotopes, ^{230}Th and ^{231}Pa, for the documenting of SR must be based on a thorough geochemical investigation of potential Eh-driven late diagenetic processes.

Despite some limitations discussed above, ^{230}Th-excess records seem to have a strong potential for shedding light on the ongoing and controversial debate about the late Pleistocene Arctic Ocean chronologies. This work should lead to a re-examination of chronostratigraphic interpretations proposed so far. Moreover, it also highlights the need to set new multi-proxy records using up to date methodologies analyzing sedimentological features and measuring physical properties, such as Be and U-series isotopes, and micropaleontological, sedimentological, geochemical, and mineralogical properties in cores recovered from different Arctic regions (i.e., the Amerasian and Eurasian basins and adjacent continental margins). Such an effort is still required to produce robust pan-Arctic core correlations to develop a coherent, multi-proxy-based chronology of Pleistocene Arctic Ocean sediments. Doing so will enable more precise paleoceanographic reconstructions, yielding an improved understanding of the role of the Arctic Ocean in the global

paleoclimate system, which is needed for paleoclimate modeling endeavors (e.g., Kageyama et al., 2021).

Data availability

All the data used in this study are available in Appendix files and through the PANGAEA database (https://doi.org/10.1594/PANGAEA.929872).

Declaration of Competing Interest

The authors declare that they have no known competing financial interests or personal relationships that could have appeared to influence the work reported in this paper.

Acknowledgments

This study is a contribution to the Germany-Canada ArcTrain program funded by the Natural Sciences and Engineering Research Council of Canada (NSERC) and the Deutsche Forschungsgemeinschaft. AdV and CHM also acknowledge support from NSERC discovery grants. Geotop laboratories are supported by the *Fonds de Recherche du Québec* (*Sciences naturelles et Technologie*). In the Geotop laboratories, support from Agnieszka Adamowicz, André Poirier, François Hardy, Jean-François Hélie, Julien Gogot, Michel Preda, and Pierre-Marc Godbout was essential for completing all the analytical work behind this study. Thanks to the Alfred Wegener Institute for providing samples and data for this study and to two anonymous reviewers whose comments helped to clarify several aspects of the present paper.

Appendix A. Supplementary data

Supplementary data to this article can be found online at https://doi.org/10.1016/j.margeo.2022.106802.

References

Allard, G., Roy, M., Ghaleb, B., Richard, P.J.H., Larouche, A.C., Veillette, J.J., Parent, M., 2012. Constraining the age of the last interglacial-glacial transition in the Hudson Bay lowlands (Canada) using U-Th dating of buried wood. Quat. Geochronol. 7, 37–47. https://doi.org/10.1016/j.quageo.2011.09.004.

Anderson, R.F., Bacon, M.P., Brewer, P.G., 1983. Removal of ^{230}Th and 231pa from the open ocean. Earth Planet. Sci. Lett. 62, 7–23.

Backman, J., Jakobsson, M., Løvlie, R., Polyak, L., Febo, L.A., 2004. Is the Central Arctic Ocean a sediment starved basin? Quat. Sci. Rev. 23, 1435–1454.

Baskaran, M., Santschi, P.H., Benoit, G., Honeyman, B.D., 1992. Scavenging of thorium isotopes by colloids in seawater of the Gulf of Mexico. Geochim. Cosmochim. Acta 56, 3375–3388. https://doi.org/10.1016/0016-7037(92)90385-V.

Behrends, M., 1999. Reconstruction of Sea-Ice Drift and Terrigenous Sediment Supply in the Late Quaternary: Heavy-mineral Associations in Sediments of the Laptev-Sea Continental Margin and the Central Arctic Ocean. Reports on Polar Research 310, 167 pp. PhD Thesis University of Bremen, German. epic.awi.de/id/eprint/26490/1/BerPolarforsch1999310.

Bonatti, E., Fisher, D.E., Joensuu, O., Rydell, H.S., 1971. Postdepositional mobility of some transition elements, phosphorus, uranium and thorium in deep sea sediments. Geochim. Cosmochim. Acta 35, 189–201. https://doi.org/10.1016/0016-7037(71)90057-3.

Broecker, W., Mix, A., Andree, M., Oeschger, H., 1984. Radiocarbon measurements on coexisting benthic and planktic foraminifera shells: potential for reconstructing ocean ventilation times over the past 20 000 years. Nucl. Inst. Methods Phys. Res. B 5, 331–339. https://doi.org/10.1016/0168-583X(84)90538-X.

Chen, J.H., Lawrence Edwards, R., Wasserburg, G.J., 1986. 238U, 234U and 232Th in seawater. Earth Planet. Sci. Lett. 80, 241–251. https://doi.org/10.1016/0012-821X(86)90108-1.

Cheng, H., Lawrence Edwards, R., Shen, C.C., Polyak, V.J., Asmerom, Y., Woodhead, J., Hellstrom, J., Wang, Y., Kong, X., Spötl, C., Wang, X., Calvin Alexander, E., 2013. Improvements in ^{230}Th dating, ^{230}Th and ^{234}U half-life values, and U-Th isotopic measurements by multi-collector inductively coupled plasma mass spectrometry. Earth Planet. Sci. Lett. 371–372, 82–91. https://doi.org/10.1016/j.epsl.2013.04.006.

Clark, D.L., 1970. Magnetic reversals and sedimentation rates in the Arctic Ocean. Geol. Soc. Am. Bull. 81 (10), 3129–3134. https://doi.org/10.1130/0016-7606.

Clark, D.L., 1981. Geology and geophysics of the Amerasian Basin. In: The Arctic Ocean. Springer, Boston, MA, pp. 599–634. https://doi.org/10.1007/978-1-4757-1248-3_12.

Clark, D.L., Whitman, R.R., Morgan, K.A., Mackey, S.D., 1980. Stratigraphy and glacial-marine sediments of the Amerasian basin, Central Arctic Ocean. Geol. Soc. Am. Sp. Pap. 181 https://doi.org/10.1130/SPE181.

Colley, S., Thomson, J., Wilson, T.R.S., Higgs, N.C., 1984. Post-depositional migration of elements during diagenesis in brown clay and turbidite sequences in the North East Atlantic. Geochim. Cosmochim. Acta 48, 1223–1235. https://doi.org/10.1016/0016-7037(84)90057-7.

Colley, S., Thomson, J., Toole, J., 1989. Uranium relocations and derivation of quasi-isochrons for a turbidite/pelagic sequence in the Northeast Atlantic. Geochim. Cosmochim. Acta 53, 1223–1234. https://doi.org/10.1016/0016-7037(89)90058-6.

Costa, K.M., Hayes, C.M., Anderson, R.F., Pavia, F., Bausch, A., et al., 2019. ^{230}Th normalization: new insights on an essential tool for quantifying sedimentary fluxes in the modern and Quaternary ocean. Paleoceanogr. Paleoclimatol. 35 (2), e2019PA003820 https://doi.org/10.1029/2019PA003820.

Dankworth, M., 2016. Hidden Diversity in Arctic Kelp Beds (Master Thesis). University of Oldenburg, Germany.

Darby, D.A., Naidu, A.S., Mowatt, T.C., Jones, G., 1989. Sediment composition and sedimentary processes in the Arctic Ocean. In: Herman, Y. (Ed.), The Arctic Seas - Climatology, Oceanography, Geology, and Biology. Springer US, New York, pp. 657–720.

Darby, D.A., Bischof, J.F., Jones, G.A., 1997. Radiocarbon chronology of depositional regimes in the western Arctic Ocean. Deep Res. Part II Top. Stud. Oceanogr. 44, 1745–1757. https://doi.org/10.1016/S0967-0645(97)00039-8.

De Vernal, A., Hillaire-Marcel, C., Le Duc, C., Roberge, P., Brice, C., Matthiessen, J., Spielhagen, R.F., Stein, R., 2020. Natural variability of the Arctic Ocean sea ice during the present interglacial. Proc. Natl. Acad. Sci. 117, 26069–26075. https://doi.org/10.1073/pnas.2008996117.

Deschamps, C.E., St-Onge, G., Montero-Serrano, J.C., Polyak, L., 2018. Chronostratigraphy and spatial distribution of magnetic sediments in the Chukchi and Beaufort seas since the last deglaciation. Boreas 47, 544–564. https://doi.org/10.1111/bor.12296.

Doell, R.R., Dalrymple, G.B., 1966. Geomagnetic Polarity Epochs : a new polarity event and the age of the Brunhes-Matuyama boundary. Science 152, 1060–1061.

Edwards, R.L., Chen, J.H., Wasserburg, G.J., 1987. ^{238}U-^{234}U-^{230}Th- ^{232}Th systematics and the precise measurement of time over the past 500,000 years. Earth Planet. Sci. Lett. 81, 175–192.

Fahl, K., Nöthig, E.M., 2007. Lithogenic and biogenic particle fluxes on the Lomonosov Ridge (Central Arctic Ocean) and their relevance for sediment accumulation: vertical vs. lateral transport. Deep Res. Part I Oceanogr. Res. Pap. 54, 1256–1272. https://doi.org/10.1016/j.dsr.2007.04.014.

Fahl, K., Stein, R., 1999. Biomarkers as organic-carbon-source and environmental indicators in the late Quaternary Arctic Ocean: "Problems and perspectives". Mar. Chem. 63, 293–309.

Farmer, J.R., Sigman, D.M., Granger, J., Underwood, O.M., Fripiat, F., Cronin, T.M., Martínez-García, A., Haug, G.H., 2021. Arctic Ocean stratification set by sea level and freshwater inputs since the last ice age. Nat. Geosci. 14, 684–689. https://doi.org/10.1038/s41561-021-00789-y.

Francois, R., Frank, M., Rutgers van der Loeff, M.M., Bacon, M.P., 2004. 230Th normalization: an essential tool for interpreting sedimentary fluxes during the late Quaternary. Paleoceanography 19, PA1018.

Frechen, M., Sierralta, M., Oezen, D., Urban, B., 2007. 8. Uranium-series dating of peat from central and Northern Europe. Dev. Quat. Sci. 7, 93–117. https://doi.org/10.1016/S1571-0866(07)80033-9.

Gariepy, C., Ghaleb, B., Hillaire-Marcel, C., Mucci, A., Vallieres, S., 1994. Early diagenetic processes in Labrador Sea sediments: uranium- isotope geochemistry. Can. J. Earth Sci. 31, 28–37. https://doi.org/10.1139/e94-004.

Geibert, W., Matthiessen, J., Stimac, I., Wollenburg, J., Stein, R., 2021. Glacial episodes of a freshwater Arctic Ocean covered by a thick ice shelf. Nature 590, 97–102. https://doi.org/10.1038/s41586-021-03186-y.

Goñi, M.A., O'Connor, A.E., Kuzyk, Z.Z., Yunker, M.B., Gobeil, C., Macdonald, R.W., 2013. Distribution and sources of organic matter in surface marine sediments across the north American Arctic margin. J. Geophys. Res. Ocean 118, 4017–4035. https://doi.org/10.1002/jgrc.20286.

Grenier, M., François, R., Soon, M., Rutgers van der Loeff, M., Yu, X., Valk, O., Not, C., Moran, S.B., Edwards, R.L., Lu, Y., Lepore, K., Allen, S.E., 2019. Changes in Circulation and Particle Scavenging in the Amerasian Basin of the Arctic Ocean over the last three decades Inferred from the Water Column distribution of Geochemical Tracers. J. Geophys. Res. Ocean 124, 9338–9363. https://doi.org/10.1029/2019JC015265.

Gusev, E.A., Maksimov, F.E., Kuznetsov, V.Y., Basov, V.A., Novikhina, E.S., Kupriyanova, N.V., Levchenko, S.B., Zherebtsov, I.E., 2013. Stratigraphy of bottom sediments in the Mendeleev Ridge area (Arctic Ocean). Dokl. Earth Sci. 450, 602–606. https://doi.org/10.1134/S1028334X13060111.

Hillaire-Marcel, C., Ghaleb, B., de Vernal, A., Maccali, J., Cuny, K., Jacobel, A., Le Duc, C., McManus, J., 2017. A new chronology of late quaternary sequences from the Central Arctic Ocean based on "Extinction Ages" of their excesses in ^{231}Pa and ^{230}Th. Geochem. Geophys. Geosyst. 18, 4573–4585. https://doi.org/10.1002/2017GC007050.

Hillaire-Marcel, C., Myers, P.G., Marshall, S., Tarasov, L., Purcell, K., Not, C., de Vernal, A., 2022. Challenging the hypothesis of an Arctic Ocean lake during recent glacial episodes. J. Quat. Sci. https://doi.org/10.1002/jqs.3421 in press.

Hoffmann, S.S., 2009. Uranium-Series Radionuclide Records of Paleoceanographic and Sedimentary Changes in the Arctic Ocean (Doctoral dissertation). Massachusetts Institute of Technology, and Woods Hole Oceanographic Institution.

Hoffmann, S.S., McManus, J.F., Curry, W.B., Susan Brown-Leger, L., 2013. Persistent export of 231 Pa from the deep Central Arctic Ocean over the past 35,000 years. Nature 497, 603–606. https://doi.org/10.1038/nature12145.
Hörner, T., Stein, R., Fahl, K., Birgel, D., 2016. Post-glacial variability of sea ice cover, river run-off and biological production in the western Laptev Sea (Arctic Ocean) - a high-resolution biomarker study. Quat. Sci. Rev. 143, 133–149. https://doi.org/10.1016/j.quascirev.2016.04.011.
Huh, C.A., Pisias, N.G., Kelley, J.M., Maiti, T.C., Grantz, A., 1997. Natural radionuclides and plutonium in sediments from the western Arctic Ocean: Sedimentation rates and pathways of radionuclides. Deep Res. Part II Top. Stud. Oceanogr. 44, 1725–1727. https://doi.org/10.1016/S0967-0645(97)00040-4.
Jakobsson, M., Lovlie, R., Al-Hanbali, H., Arnold, E., Backman, J., Mörth, M., 2000. Manganese and color cycles in Arctic Ocean sediments constrain Pleistocene chronology. Geology 28, 23–26. https://doi.org/10.1130/0091-7613(2000)28.
Jakobsson, M., et al., 2012. The International Bathymetric Chart of the Arctic Ocean (IBCAO) version 3.0. Geophys. Res. Lett. 39, 1–6. https://doi.org/10.1029/2012GL052219.
Kageyama, M., et al., 2021. The PMIP4-CMIP6 last Glacial Maximum experiments: preliminary results and comparison with the PMIP3-CMIP5 simulations. Clim. Past 17, 1065–1089. https://doi.org/10.5194/cp-2019-169.
Kigoshi, K., 1971. Alpha-recoil thorium-234: dissolution into water and the uranium-234/uranium-238 disequilibrium in nature. Science 173 (3991), 47–48.
Kipp, L.E., McManus, J.F., Kienast, M., 2021. Radioisotope constraints of Arctic deep water export to the North Atlantic. Nat. Commun. 12 https://doi.org/10.1038/s41467-021-23877-4.
Kleman, J., Applegate, P.J., 2014. Durations and propagation patterns of ice sheet instability events. Quat. Sci. Rev. 92, 32–39. https://doi.org/10.1016/j.quascirev.2013.07.030.
Ku, T.L., Broecker, W.S., 1965. Rates of sedimentation in the Arctic Ocean. Prog. Oceanogr. 4, 95–104. https://doi.org/10.1016/0079-6611(65)90043-1.
Kutscher, L., Mörth, C.M., Porcelli, D., Hirst, C., Maximov, T.C., Petrov, R.E., Andersson, P.S., 2017. Spatial variation in concentration and sources of organic carbon in the Lena River, Siberia. J. Geophys. Res. Biogeosci. 122, 1999–2016. https://doi.org/10.1002/2017JG003858.
Lara, R.J., Rachold, V., Kattner, G., Hubberten, H.W., Guggenberger, G., Skoog, A., Thomas, D.N., 1998. Dissolved organic matter and nutrients in the Lena River, Siberian Arctic: characteristics and distribution. Mar. Chem. 59, 301–309. https://doi.org/10.1016/S0304-4203(97)00076-5.
Łokas, E., Zaborska, A., Sobota, I., Gaca, P., Milton, J.A., Kocurek, P., Cwanek, A., 2019. Airborne radionuclides and heavy metals in high Arctic terrestrial environment as the indicators of sources and transfers of contamination. Cryosphere 13, 2075–2086. https://doi.org/10.5194/tc-13-2075-2019.
Löwemark, L., März, C., O'Regan, M., Gyllencreutz, R., 2014. Arctic Ocean Mn-stratigraphy: genesis, synthesis and inter-basin correlation. Quat. Sci. Rev. 92, 97–111. https://doi.org/10.1016/j.quascirev.2013.11.018.
Maccali, J., Hillaire-Marcel, C., Carignan, J., Reisberg, L.C., 2013. Geochemical signatures of sediments documenting Arctic Sea-ice and water mass export through Fram Strait since the last Glacial Maximum. Quat. Sci. Rev. 64, 136–151. https://doi.org/10.1016/j.quascirev.2012.10.029.
Macdonald, R.W., Gobeil, C., 2012. Manganese sources and sinks in the Arctic Ocean with reference to periodic enrichments in basin sediments. Aquat. Geochem. 18, 565–591. https://doi.org/10.1007/s10498-011-9149-9.
Matthiessen, J., Knies, J., Nowaczyk, N.R., Stein, R., 2001. Late Quaternary dinoflagellate cyst stratigraphy at the Eurasian continental margin, Arctic Ocean: Indications for Atlantic water inflow in the past 150,000 years. Glob. Planet. Chang. 31, 65–86. https://doi.org/10.1016/S0921-8181(01)00113-8.
Müller, C., 1999. Reconstruction of Paleoenvironmental Conditions at the Laptev Sea Continental Margin during the Last Two Glacial/Interglacial Cycles Based on Sedimentological and Mineralogical Investigations. Reports on Polar 328, 146 pp. PhD Thesis University of Bremen, German. epic.awi.de/id/eprint/26507/1/BerPolarforsch1999328.
Müller, C., Stein, R., 2000. Sedimentology of core PS2757-8. PANGEA Data. https://doi.org/10.1594/PANGAEA.57243.
Müller-Lupp, T., Bauch, H.A., Erlenkeuser, H., Hefter, J., Kassens, H., Thiede, J., 2000. Changes in the deposition of terrestrial organic matter on the Laptev Sea shelf during the Holocene: evidence from stable carbon isotopes. Int. J. Earth Sci. 89, 563–568.
Naidu, A.S., Cooper, L.W., Finney, B.P., Macdonald, R.W., Alexander, C., Semiletov, I.P., 2000. Organic carbon isotope ratio ($\delta^{13}C$) of Arctic Amerasian Continental shelf sediments. Int. J. Earth Sci. 89, 522–532. https://doi.org/10.1007/s005310000121.
Niessen, F., 1996. Physical properties of sediment core PS2757-8. PANGEA Data. https://doi.org/10.1594/PANGAEA.50569.
Nørgaard-Pedersen, N., Spielhagen, R.F., Erlenkeuser, H., Grootes, P.M., Heinemeier, J., Knies, J., 2003. Arctic Ocean during the last Glacial Maximum: atlantic and polar domains of surface water mass distribution and ice cover. Paleoceanography 18, 1–19. https://doi.org/10.1029/2002pa000781.
Not, C., Hillaire-Marcel, C., 2010. Time constraints from ^{230}Th and ^{231}Pa data in late Quaternary, low sedimentation rate sequences from the Arctic Ocean: an example from the northern Mendeleev Ridge. Quat. Sci. Rev. 29, 3665–3675. https://doi.org/10.1016/j.quascirev.2010.06.042.
Nowaczyk, N.R., Baumann, M., 1992. Combined high-resolution magnetostratigraphy and nannofossil biostratigraphy for late Quaternary Arctic Ocean sediments. Deep-Sea Res. 39, 567–601.
Nowaczyk, N.R., Frederichs, T.W., Eisenhauer, A., Gard, G., 1994. Magnetostratigraphic data from late quaternary sediments from the Yermak Plateau, Arctic Ocean: evidence for four geomagnetic polarity events within the last 170 ka of the Brunhes Chron. Geophys. J. Int. 117, 453–471. https://doi.org/10.1111/j.1365-246X.1994.tb03944.x.
O'Regan, M., King, J., Backman, J., Jakobsson, M., Pälike, H., Moran, K., Heil, C., Sakamoto, T., Cronin, T.M., Jordan, R.W., 2008. Constraints on the Pleistocene chronology of sediments from the Lomonosov Ridge. Paleoceanography 23, 1–18. https://doi.org/10.1029/2007PA001551.
O'Regan, M., Backman, J., Fornaciari, E., Jakobsson, M., West, G., 2020. Calcareous nannofossils anchor chronologies for Arctic Ocean sediments back to 500 ka. Geology 48 (11), 1115–1119. https://doi.org/10.1130/G47479.1.
Paul, D., White, W.M., Turcotte, D.L., 2003. Constraints on the 232Th/238U ratio (K) of the continental crust. Geochem. Geophys. Geosyst. 4 https://doi.org/10.1029/2002GC000497.
Pavia, F.J., Anderson, R.F., Pinedo-Gonzalez, P., Fleisher, M.Q., Brzezinski, M.A., Robinson, R.S., 2020. Isopycnal Transport and Scavenging of ^{230}Th and ^{231}Pa in the Pacific Southern Ocean. Glob. Biogeochem. Cycles 34, 1–16. https://doi.org/10.1029/2020GB006760.
Polyak, L., Curry, W.B., Darby, D.A., Bischof, J., Cronin, T.M., 2004. Contrasting glacial/interglacial regimes in the western Arctic Ocean as exemplified by a sedimentary record from the Mendeleev Ridge. Palaeogeogr. Palaeoclimatol. Palaeoecol. 203, 73–93. https://doi.org/10.1016/S0031-0182(03)00661-8.
Polyak, L., Bischof, J., Ortiz, J.D., Darby, D.A., Channell, J.E.T., Xuan, C., Kaufman, D.S., Løvlie, R., Schneider, D.A., Eberl, D.D., Adler, R.E., Council, E.A., 2009. Late Quaternary stratigraphy and sedimentation patterns in the western Arctic Ocean. Glob. Planet. Chang. 68, 5–17. https://doi.org/10.1016/j.gloplacha.2009.03.014.
Poore, R.Z., Osterman, L., Curry, W.B., Phillips, R.L., 1999. Late Pleistocene and Holocene meltwater events in the western Arctic Ocean. Geology 27 (8), 759–762.
Rachor, E., 1997. Scientific Cruise Report of the Arctic Expedition ARK-XI11 of RV "Polarstern" in 1995: (German-Russian Project LADI: Laptev Sea-Arctic Deep Basin Interrelations). Alfred-Wegener-Inst. für Polar-und Meeresforschung. Ber, Polarforsch, p. 226.
Ravelo, A.C., Hillaire-Marcel, C., 2007. The use of oxygen and carbon isotopes of foraminifera in paleoceanography. In: Hillaire-Marcel, C., de Vernal, A. (Eds.), Proxies in Late Cenozoic Paleoceanography. Developments in Marine Geology, Elsevier, Amsterdam, pp. 735–764.
Roy-Barman, M., Jeandel, C., Souhaut, M., van der Loeff, M.R., Voege, I., Leblond, N., Freydier, R., 2005. The influence of particle composition on thorium scavenging in the NE Atlantic Ocean (POMME experiment). Earth Planet. Sci. Lett. 240, 681–693. https://doi.org/10.1016/j.epsl.2005.09.059.
Schirrmeister, L., Oezen, D., Geyh, M.A., 2002. 230Th/U dating of frozen peat, Bol'shoy Lyakhovsky Island (northern Siberia). Quat. Res. 57, 253–258. https://doi.org/10.1006/qres.2001.2306.
Schoster, F., 2005. Geochemistry of sediment core PS2757-8. PANGEA Data. https://doi.org/10.1594/PANGAEA.227863.
Siddall, M., Rohling, E.J., Thompson, W.G., Waelbroeck, C., 2008. Marine isotope stage 3 sea level fluctuations: Data synthesis and new outlook. Rev. Geophys. 46, RG4003. https://doi.org/10.1029/2007RG000226.
Spell, T.L., Mcdougall, I., 1992. Revisions to the ages of the Brunhes - Matuyama boundary and the Pleistocene geomagnetic polarity timescale. Geophys. Res. Lett. 19, 1181–1184.
St. John, K., 2008. Cenozoic ice-rafting history of the Central Arctic Ocean: terrigenous sands on the Lomonosov Ridge. Paleoceanography 23, 1–12. https://doi.org/10.1029/2007PA00148.
Stein, R., 2008. The stratigraphic framework of Arctic Ocean sediment cores: background, problems, and perspectives. In: Stein, R. (Ed.), Arctic Ocean Sediments: Processes, Proxies, and Palaeoenvironment, Dev. Mar. Geol. 2, pp. 287–316.
Stein, R., Fahl, K., 2004. The Laptev Sea: distribution, sources, variability and burial of organic carbon. In: Stein, R., Macdonald, R.W. (Eds.), The Organic Carbon Cycle in the Arctic Ocean. Springer Verlag, Heidelberg, pp. 213–237.
Stein, R., Macdonald, R.W., 2004. The central Arctic Ocean: distribution, sources, variability and burial of organic carbon. In: Stein, R., Macdonald, R.W. (Eds.), The Organic Carbon Cycle in the Arctic Ocean. Springer-Verlag, Heidelberg, pp. 24–32.
Stein, R., Matthiessen, J., Niessen, F., Krylov, A., Sung-Il, N., Bazhenova, E., 2010. Towards a Better (Litho-) Stratigraphy and Reconstruction of Quaternary Paleoenvironment in the Amerasian Basin (Arctic Ocean). Polarforschung 79 (2), 97–121.
Stein, R., Schubert, C.J., Vogt, C., Fütterer, D., 1994. Stable isotope stratigraphy, sedimentation rates, and salinity changes in the latest Pleistocene to Holocene eastern Central Arctic Ocean. Mar. Geol. 119, 333–355.
Stein, R., Behrends, M., Spielhagen, R., 1997. Lithostratigraphy and sediment characteristics. In: Rachor, E. (Ed.), Scientific Cruise Report of the Arctic Expedition ARK-XI/1 of RV "Polarstern" in 1995, Rep. Polar Res. 226, pp. 143–152 epic.awi.de/id/eprint/26404/1/BerPolarforsch1997226.
Stein, R., Boucsein, B., Fahl, K., Garcia de Oteyza, T., Knies, J., Niessen, F., 2001a. Accumulation of particulate organic carbon at the Eurasian continental margin during late Quaternary times: Controlling mechanisms and paleoenvironmental significance. Glob. Planet. Chang. 31 (1–4), 87–102.
Stein, R., Boucsein, B., Fahl, K., Garcia de Oteyza, T., Knies, J., Niessen, F., 2001b. Total organic carbon, nitrogen and calcium carbonate of sediment core PS2757-8. PANGAEA. https://doi.org/10.1594/PANGAEA.137047.
Stein, R., Fahl, K., Gierz, P., Niessen, F., Lohmann, G., 2017a. Arctic Ocean sea ice cover during the penultimate glacial and the last interglacial. Nat. Commun. 8, 373. www.nature.com/articles/s41467-017-00552-1.
Stein, R., Fahl, K., Schade, I., Manerung, A., Wassmuth, S., Niessen, F., Nam, S. Il, 2017b. Holocene variability in sea ice cover, primary production, and Pacific-Water inflow and climate change in the Chukchi and East Siberian Seas (Arctic Ocean). J. Quat. Sci. 32, 362–379. https://doi.org/10.1002/jqs.2929.

Strobl, C., 1998. Datierung von Sedimentkernen und Rekonstruktion der Transportwege der Radionuklide ^{10}Be, ^{230}Th und ^{231} Pa in hohen nördlichen Breiten (Doctoral dissertation). Universität Heidelberg, 183 p. & Appendix.

Thomson, J., Higgs, N.C., Wilson, T.R.S., Croudace, I.W., De Lange, G.J., Van Santvoort, P.J.M., 1995. Redistribution and geochemical behaviour of redox-sensitive elements around S1, the most recent eastern Mediterranean sapropel. Geochim. Cosmochim. Acta 59, 3487–3501. https://doi.org/10.1016/0016-7037(95)00232-O.

Vallières, S., 1997. Flux d'uranium et excès de ^{230}Th dans les sédiments de la Mer du Labrador — Relation avec les conditions paléocéanographiques et la paléoproductivité du bassin. PhD thesis. Université du Québec à Montréal, Montréal (QC), Canada, 144 p.

Vallières, S., Hillaire-Marcel, C., Ghaleb, B., 1993. Déséquilibres U/Th dans les dépôts meubles des Basses-Terres du Saint-Laurent, Québec. Can. J. Earth Sci. 30, 1730–1740.

Veiga-Pires, C., Hillaire-Marcel, C., 1999. U and Th isotope constraints on the duration of Heinrich events H0-H4 in the southeastern Labrador Sea. Paleoceanography 14, 187–199.

Viers, J., Dupré, B., Gaillardet, J., 2009. Chemical composition of suspended sediments in World Rivers: New insights from a new database. Sci. Total Environ. 407, 853–868. https://doi.org/10.1016/j.scitotenv.2008.09.053.

Wang, Z., Lee, S.W., Catalano, J.G., Lezama-Pacheco, J.S., Bargar, J.R., Tebo, B.M., Giammar, D.E., 2013. Adsorption of uranium(VI) to manganese oxides: X-ray absorption spectroscopy and surface complexation modeling. Environ. Sci. Technol. 47, 850–858. https://doi.org/10.1021/es304454g.

West, G., Alexanderson, H., Jakobsson, M., O'Regan, M., 2021. Optically stimulated luminescence dating supports pre-Eemian age for glacial ice on the Lomonosov Ridge off the East Siberian continental shelf. Quat. Sci. Rev. 267, 107082 https://doi.org/10.1016/j.quascirev.2021.107082.

Wycech, J., Clay Kelly, D., Marcott, S., 2016. Effects of seafloor diagenesis on planktic foraminiferal radiocarbon ages. Geology 44, 551–554. https://doi.org/10.1130/G37864.1.

Xuan, C., Channell, J.E.T., Polyak, L., Darby, D.A., 2012. Paleomagnetism of Quaternary sediments from Lomonosov Ridge and Yermak Plateau: implications for age models in the Arctic Ocean. Quat. Sci. Rev. 32, 48–63.

Zhang, J., Li, S.H., 2020. Review of the post-IR IRSL dating protocols of K-Feldspar. Meth. Protoc. 3 (1), 7. https://doi.org/10.3390/mps3010007.

Ziemen, F.A., Kapsch, M.-L., Klockmann, M., Mikolajewicz, U., 2019. Heinrich events show two-stage climate response in transient glacial simulations. Clim. Past 15, 153–168. https://doi.org/10.5194/cp-15-153-2019.